Microchemical Journal 156 (2020) 104811

Contents lists available at ScienceDirect

Microchemical Journal

journal homepage: www.elsevier.com/locate/microc

Identification of green pigments and binders in late medieval painted wings from Norwegian churches

Elena Platania[a,b,*], Noëlle L.W. Streeton[b], Anna Lluveras-Tenorio[c,*], Anna Vila[d,e], David Buti[d], Francesco Caruso[b,f], Hartmut Kutzke[g], Arne Karlsson[a,h], Maria Perla Colombini[d], Einar Uggerud[a]

[a] Hylleraas Centre for Quantum Molecular Sciences, Department of Chemistry, University of Oslo, Post Box 1033 Blindern, 0315 Oslo, Norway
[b] Conservation Studies, Department of Archaeology, Conservation and History, University of Oslo, Post Box 1008 Blindern, 0315 Oslo, Norway
[c] Laboratory of Chemical Science for Safeguarding the Cultural Heritage, Department of Chemistry and Industrial Chemistry, University of Pisa, Via Risorgimento 35, 56126 Pisa, Italy
[d] Statens Museum for Kunst, Centre for Art Technological Studies and Conservation, Sølvgade 48, 50, 1307 Copenaghen, Denmark
[e] Fundació "la Caixa", Collection Department, CaixaForum Barcelona, Av. Francesc Ferrer i Guàrdia, 6-8, 08038 - Barcelona
[f] Department of Art Technology, Swiss Institute for Art Research (SIK-ISEA), Zollikerstrasse 32, 8032 Zurich, Switzerland
[g] Museum of Cultural History, University of Oslo, St. Olavs plass, 0130 Oslo, Norway
[h] SINTEF Industri, Prosessteknologi, Post Box 124 Blindern, 0314 Oslo, Norway

ARTICLE INFO

Keywords:
Copper-green pigments
Cross-sections
Metal soaps
Binders
Late medieval
Paint delamination

ABSTRACT

Green pigments in micro-samples taken from three late-medieval painted objects from Norwegian churches have been investigated with the aim to characterize their constituents and understand how they relate to damages observed in passages containing green paints. The cross-sections were analyzed by optical microscopy under visible and UV light, Scanning Electron Microscopy coupled with Energy Dispersive X-Ray Spectrometry and vibrational spectroscopies (Raman, ATR-FTIR). In addition, Gas Chromatography coupled with Mass Spectrometry was employed for the characterization of binding media, using a derivatization methodology recently developed for the detection of metal soaps in paint samples. This extensive characterization aided the identification of the individual constituents and the stratigraphy of green paints. It also builds the foundation for future ageing studies that can provide better insights into the mechanisms of the processes at stake in selective delamination of paints containing copper complexes.

1. Introduction

1.1. Detection and identification of copper-based pigments in late medieval paint samples

Northern European painters active in the 15th and 16th centuries made extensive use of neutral or basic copper acetates [1,2]. These green compounds are corrosion products obtained by exposing copper plates, strips or foils to different acidic substances. Of these substances, vinegar seems to have been most common, although curdled milk, ammonium salts, honey and wine lees could have also been used [1,3]. These copper compounds are described by the umbrella term "verdigris", but differ from each other in terms of manufacturing procedures and purification, degradation patterns, and coordination environment of Cu(II) [3–7]. For these reasons, among others, the analysis and identification of such copper complexes in paint samples is challenging. In fact, despite the large number of articles on the reproduction of varieties of verdigris [3–5,8–11], it is not always possible to identify unambiguously the type of copper-based pigment found in a paint sample.

1.2. Issues in the analysis of aged verdigris paint

A common problem encountered during measurements of heritage objects with Raman Spectroscopy is interference from the fluorescence of aged samples [12]. Moreover, the interaction between the copper-based pigment – often found in mixture with other pigments – and the organic binder, together with the dynamic alteration of components in the paint, affects both the detection and the recognition of the copper compound, thus complicating analyses [13]. In addition, it has been observed in paint samples from art objects that pigments identified as verdigris, when mixed with proteinaceous and lipidic binders, tend to lose their crystallinity over time [14]. Identification of these compounds in paint samples by Attenuated Total Reflectance (ATR)-FTIR

* Corresponding authors.
E-mail addresses: elenaplatania@kjemi.uio.no (E. Platania), alluverastenorio@gmail.com (A. Lluveras-Tenorio).

https://doi.org/10.1016/j.microc.2020.104811
Received 26 November 2019; Received in revised form 11 February 2020; Accepted 8 March 2020
Available online 10 March 2020
0026-265X/ © 2020 The Authors. Published by Elsevier B.V. This is an open access article under the CC BY license (http://creativecommons.org/licenses/BY/4.0/).

has been particularly difficult when verdigris and lead-based pigments (such as lead-tin yellow type I ($PbSnO_4$), lead white ($2PbCO_3{\cdot}Pb(OH)_2$) and red lead (Pb_3O_4) [15]) are present. In fact, characteristic infrared absorption bands for lead-based pigments (and some of their degradation products) are in the same region as those for verdigris [13]. In light of these considerations, the adoption of a multi-analytical approach is critical for a comprehensive characterization and detection of complex mixtures of compounds in paint samples. The application of complementary Raman and FTIR spectroscopies is fundamental in identifying signature compounds in synthetic copper-based greens [11]. While FTIR is a powerful technique for the investigation of organic compounds, Raman spectroscopy, allows for an extensive identification of several classes of pigments (both organic and inorganic) dispersed in different binders [2,16,17]. In addition, in presence of metal carboxylates, FTIR is able to identify the metal cation coordinated to the carboxylate group. On the other hand, Raman spectroscopy allows to distinguish the carbon chain length of the carboxylate species [10]. Such analytical tools are further strengthened when combined with imaging [18], chromatography [19,20] and/or diffraction [21] techniques, leading to a more complete characterization of the artistic materials and their related degradation processes.

1.3. Case studies

The Museum of Cultural History (KHM) of the University of Oslo owns a large collection of late medieval objects from Norwegian churches, which have been studied as part of the interdisciplinary project "After the Black Death: Painting and Polychrome Sculpture in Norway 1350-1550" (henceforth "ABD") [22–25]. Most objects belonging to this collection are either substantially or profoundly damaged. In some locations, the green passages have delaminated selectively, whereas red or blue passages remain intact. Although the ground layers that were under green paints are often still preserved (Fig. 1A), more often these have been worn away or been removed to reveal the wooden support, to reduce the visual disruption of the loss (Figs. 1A and B). The green passages in a number of objects have been investigated. All contain copper-based pigments. The majority of these passages are in poor condition with diffuse flaking, but curiously have rarely turned brown, as is often the case with copper-based green pigments [12,26,27].

From a set of pre-existing and new paint cross-sections from regions where green paints were partially delaminated, three representative samples constitute the main topic of this work. These include micro-samples from three painted wings from Norwegian churches (Fig. 1), which interestingly share a common workshop pattern [22].

Analyses of these samples aimed firstly to establish similarities and differences between the green paints used in these works – two of which were produced in the second half of 15th century while the third was probably painted in the first decade of 16th century [28]. Identification of pigments, binding media and paint stratigraphies were important to form a foundation for paint reconstructions. Weathering experiments will be designed in the future to lend insight into the physical and chemical causes for flaking and delamination.

For this study, cross-sections were analyzed with optical microscopy under UV and visible light, Scanning Electron Microscopy coupled with Energy Dispersive X-Ray Spectrometry (SEM-EDX), Raman Spectroscopy, ATR-FTIR and Gas Chromatography coupled with Mass Spectrometry (GC-MS). In addition, a recently developed GC-MS method [29,30] was applied for the detection of mixtures of free fatty acids and metal soaps, which supported Raman and ATR-FTIR results. The analytical strategy adopted in this study, based on the application of complementary vibrational spectroscopies and empowered by advanced gas chromatographic methods, was successful for the identification of both pigments and binders in complex paint samples from late medieval objects from Norwegian churches.

2. Materials and methods

2.1. Cross-sections preparation

Representative sample areas were identified during preliminary investigations with a portable X-Ray Fluorescence analyzer (Thermo Fisher Scientific, Oslo, Norway) and, thereafter, three micro-fragments were taken with a scalpel from edges of existing losses (see Fig. 1). Fragments were embedded in acrylic Technovit 2000 LC resin (Heraeus-Kulzer GmbH & Co. KG, Hanau, Germany) and mounted in Easy-

Fig. 1. Painted wings from (A) the shrine from Bygland (Aust-Agder); (B) the altarpiece from Skjervøy (Troms); (C) and shrine (now lost) from Røldal (Hordaland), inv. nos. C6113, C3000, and C5067 respectively (images © Kirsten Jensen Helgeland, KHM, University of Oslo). Locations for samples L33_31 (A), L175_8 (B), and L176_12 (C) are marked with white arrows and shown in macro-images (images © N.L.W. Streeton and ABD project).

Section sample holders (VWFecit, London, UK). The resin was polymerized at 90 °C under blue light (440 nm) emitted by the Technotray CU polymerization unit (Heraeus-Kulzer GmbH & Co. KG, Hanau, Germany), for 10 min and left to set overnight at room temperature. Embedded samples were polished first on a rotary polisher (Lab-Pol5 instrument from Struers, Ballerup, Denmark) and then hand-polished with MicroMesh (GC Abrasives, Darlington, UK) polishing cloths by increasing progressively the grit (from 500 to 12,000 mesh/in) of the cloth.

2.2. Analytical instrumentation and methods

2.2.1. Light microscopy

Dark field reflected light photomicrographs were acquired on a Leica DM LM microscope (Leica Microsystems GmbH, Wetzlar, Germany) equipped with different lenses (5×, 10×, 20×, 50×). Visible and UV light were respectively provided by a 100 W halogen projection lamp and an external light source for fluorescence excitation (301-185 also from Leica). Photomicrographs of the cross-sections were taken with an Olympus UC30 (Olympus Corporation, Tokyo, Japan) microscope digital camera (3.2 megapixels resolution) and processed with the Stream Motion software by Olympus.

2.2.2. Scanning electron microscopy coupled with energy dispersive X-Ray spectroscopy (SEM-EDX)

Elemental analysis and maps were obtained with a Hitachi S-3400N scanning electron microscope (Hitachi High-Technologies Global, Tokyo, Japan) (3 nm resolution in high vacuum mode, eucentric stage, backscattered electron and EDX detectors) equipped with Bruker EDX spectroscopy detection system, all operated under variable pressure vacuum (30 Pa). Measurements were carried out using 20 kV accelerating voltage and 10 mm working distance.

2.2.3. Raman spectroscopy

The Raman spectra were acquired with a Jobin-Yvon Horiba T64000 instrument (Horiba Scientific, Edison, NJ, USA) working in single/micro configuration. The backscattered light was collected through 50× objective (Thorlabs, Inc., Mölndal, Sweden), a confocal pinhole of 100 μm and a slit adjusted to a width of 100 μm. The detector was a Back Illuminated Deep Depletion CCD with a chosen active zone of 990 pixels × 25 pixels of the size 26 × 26 μm^2 mounted on the spectrograph with a focal length of 64 cm. A grating with 1800 lines/mm thus resulted in a spectral resolution ranging from 2.25 cm^{-1} in the low frequency region to 1.28 cm^{-1} in the high frequency one (around 3500 cm^{-1}). The spectra were acquired in extended range mode with 500 pixels overlap. The applied laser was a Spectra-Physics Millennia Pro SJ12 Nd:YVO_4 (Spectra Physics, Santa Clara, CA, USA) yielding 200 mW of the second harmonic generation light with a wavelength of 370 nm. This was damped by use of neutral-density filters to a power of 0.5 mW measured on the sample. Raman spectra were also collected using a confocal Raman micro-spectrometer system (InVia Renishaw, Renishaw, Wotton-under-Edge, UK). A grating of 1800 lines was used with a spectral resolution of 2 cm^{-1}. The excitation wavelength adopted for analyses was a diode laser at 785 nm. Spectral collection was made by means of a 50× objective (Leica) with a spatial resolution of the order of 3 μm. Laser power on the sample was of the order of 1 mW. The acquisition time was of 60 s with 30 accumulations. Spectra were collected using the Wire 4.2 software provided by Renishaw.

2.2.4. Infrared spectroscopy

FTIR analyses were performed with a Bruker Tensor 24 spectrometer (Bruker, Billerica, MA, USA) coupled to a Hyperion 3000 microscope equipped with a cryogenic mercury-cadmium telluride (MCT) and a focal plan array (FPA) detectors. Measurements were performed in ATR mode with a 20× objective germanium crystal with a refractive index of 4.01. The latter has an anvil design with an 80 μm tip. When the MCT detector was used, 64 averaged spectra for both the sample and the background measurements with a range of 600–4000 cm^{-1} were acquired, whereas 64 scans were taken with the FPA detector throughout the accumulation range of 900–3600 cm^{-1} with a spectral resolution of 4 cm^{-1}. Spectra were acquired using the OPUS 7.2 FTIR software by Bruker and an atmospheric compensation was applied when necessary.

2.2.5. Gas chromatography – mass spectrometry and multivariate data analysis

A GC-MS procedure was undertaken to identify polysaccharide, proteinaceous, glycerolipidic materials, as well as waxes and terpenoid resins in the same micro-sample. The procedure is based on a multistep chemical pre-treatment of the sample, in order to obtain three different fractions to be analyzed separately by GC-MS: an amino acidic, a saccharide and a lipid-resinous fractions [31–33]. Briefly, the analytical procedure is based on the ammonia extraction of proteins and polysaccharide materials from the sample in order to separate them from lipid and resinous materials. Proteinaceous and polysaccharide fractions are separated by a monolithic sorbent tip featuring a C4 stationary phase. Lipids and resins were subjected to saponification. In this way, three fractions were generated and analyzed separately by GC-MS, enabling a quantitative analysis of the components in each fraction. The detailed operating conditions and analytical procedure are described elsewhere [31–33]. Sub-sampling was manually performed on samples L175_8 and L33_31 with a scalpel under the stereomicroscope. Two subsamples from each sample were obtained corresponding to the top paint layers (L33_31_green and L175_8_green) and the preparation layer (L33_31_prep and L175_8_prep). Sub-sampling was not performed on sample L176_12 due to the very small size of the sample. Samples analyzed by GC-MS had masses between 0.1 and 0.5 mg.

A 6890N GC System by Agilent Technologies (Palo Alto, CA, USA), equipped with a programmed temperature vaporization injector and coupled with a single quadrupole mass spectrometer, 5975 Mass Selective Detector (also by Agilent) was used. The electron impact (EI) positive mode (70 eV) was used for operation and the MS transfer line temperature was 280 °C, the MS ion source temperature was kept at 230 °C and the MS quadruple temperature was at 150 °C. For the gas chromatographic separation, an HP-5MS fused silica capillary column (5% diphenyl-95% dimethylpolysiloxane, 30 m × 0.25 mm i.d., 0.25 μm film thickness, J&W Scientific, Agilent) coupled with a deactivated silica precolumn (2 m × 0.32 mm i.d., J&W Scientific, Agilent) using a quartz press fit was used.

A GC-MS method that allows the qualitative and quantitative characterization of mixtures of terpenoid acids, aliphatic mono- and dicarboxylic acids and their metal (Na, Mg, Al, Mn, Co, Cu, Zn, Cd, Pb) carboxylates in the same sample was also applied to the bulk samples containing all the paint layers. This is based on a two-step approach entailing the subsequent use of two silylating agents: 1,1,1-Trimethyl-N-(trimethylsilyl)silanamine (commonly known as hexamethyldisilazane, HMDS) and trimethylsilyl 2,2,2-trifluoro-N-trimethylsilylethanimidate (N,O-Bis(trimethylsilyl)trifluoroacetamide, BSTFA) [29,30]. The procedure is based on the selective ability of the two derivatizing agents to silylate free fatty acids and their carboxylates.

The quantitative evaluation of the data, based on the calibration curves obtained from the Selected Ions Monitoring (SIM) chromatograms, the ions chosen for the SIM acquisition, as well as the values of the limits of detection (LOD) and quantification (LOQ) for each fraction, can be found in the Supplementary Material.

Proteinaceous materials were identified on the basis of the normalized amino acid content of the samples. The latter was subjected to a multivariate statistical analysis together with a dataset of 121 reference samples of animal glue, egg and casein using the Principal Component Analysis (PCA) method [32,34–39]. Principal components (PCs) were computed using XLSTAT 6.0 (Addinsoft, Inc, New York, NY) on the correlation matrix of the raw data. Further details, as well as the

Table 1
Techniques used and samples analyzed for the characterization of the stratigraphies of the studied samples from the three late-medieval painted objects from Norwegian churches. Layer numbers correspond to those in Fig. 2.

Sample	Paint layer	Optical Microscopy	SEM-EDX	ATR-FTIR	Raman	GC-MS
L33_31	8	✓	–	–	–	–
	7	✓	✓	✓	✓	✓
	6	✓	✓	✓	✓	
	5	✓	–	–	–	
	4	✓	✓	✓	✓	
	3	✓	✓	✓	✓	
	2	–	–	–	–	–
	1	✓	✓	✓	✓	✓
L175_8	5	✓	–	–	–	✓
	4	✓	✓	✓	✓	
	3	✓	✓	✓	✓	
	2	✓	–	–	–	–
	1	✓	✓	✓	✓	✓
L176_12	6	–	–	–	–	✓
	5	✓	✓	✓	✓	
	4	✓	✓	✓	✓	
	3	✓	✓	✓	✓	
	2	✓	✓	✓	✓	
	1	✓	✓	✓	✓	

score and loading plots of the PCA, are provided in the supplementary material (Figure S12). A microwave digestion rotor MLS-1200 MEGA (Milestone Microwave Laboratory System, Sorisole (BG), Italy) with Exhaust Module EM-45/A was used for the hydrolysis of proteins and polysaccharides and the saponification of glycerolipid, waxy and resinous material.

3. Results and discussion

Table 1 shows which technique was used for analyzing the samples.

3.1. Paint stratigraphy

Cross-sections were examined first with an optical microscope to investigate the paint stratigraphy of the samples. Fig. 2 shows the micrographs taken under visible and UV light, alongside graphic representations of the cross-sections to illustrate their stratigraphies.

SEM-EDX, Raman and ATR-FTIR analyses supported the interpretation that all ground layers are based on calcium carbonate (Figure S1). The backscattered SEM micrographs showed the presence of calcareous nano-fossils, which are the main constituents of chalk [40]. Raman bands of calcium carbonate were found at 282, 711 and 1082 cm^{-1}, whereas the corresponding ATR-FTIR frequencies (Figure S2) were detected at 711, 871, 1400 and 2512 cm^{-1} [41]. The dominant absorption band centered at 1400 cm^{-1} is related to the CO_3^{2-} group [42]. Absorption bands were also identified by the C=O stretch at 1730 cm^{-1} and the weak CH stretches at 2850 and 2925 cm^{-1} [42], which indicate the possible presence of a drying oil in the ground layer, probably absorbed from the paint [43].

Raman spectra recorded from layer 3 and 4 of cross-section L33_31 (Fig. 2C) show characteristic features at 129, 196, 275, 379, 457, 480 cm^{-1}, which point to lead-tin yellow type I (Pb_2SnO_4). The three Raman bands at 255, 282 and 343 cm^{-1} [41] suggest that the small red inclusions are vermilion (HgS) and are homogeneously distributed across the whole yellow layer (Figure S3). The presence of an orange layer under a green layer points to the panel being prepared to be gilded, but instead was painted with a landscape.

In layer 2 of cross section L175_8 (Fig. 2D, E, F), light blue particles are distributed throughout a white layer. SEM-EDX elemental maps collected for the same layer show a uniform distribution of both lead and copper in the white layer (Figure S4). The characteristic Raman peak for lead white was found at 1050 cm^{-1}, whereas Raman frequencies for azurite are located respectively at 400, 539, 740, 762, 837, 1091, 1430, 1460 and 1578 cm^{-1} (Figure S5), as reported in the literature [41]. Interestingly, the SEM-EDX elemental maps of layer 2 of sample L175_8, highlight the presence of phosphorus (Figure S6), which could point to a proteinaceous binder with egg yolk [14,44]. The identification of such compounds might indicate the presence of mixed-media, used to achieve perhaps more matte visual effects, potentially to hasten drying, and create crisper lines than those produced with linseed oil alone.

The Raman spectrum (Figure S7) collected from layer 5 of cross-section L176_12 showed the characteristic spectral features for lead-tin yellow type I, mixed with lead white. In this paint layer, the UV fluorescent particles distributed across the whole layer would indicate the presence of lead carboxylates [45,46]. Unfortunately, in either Raman and ATR-FTIR spectra it is difficult to discriminate the bands associated to the metal carboxylates. Especially due to the overlap of peaks in the fingerprint area, absorption bands related to lead carboxylates were not easy to discriminate, except the band at 1539 cm^{-1}, which can be attributed to the asymmetric stretching vibration of the COO^- group of these compounds [42,47].

3.2. Investigation of the green pigments

The Raman spectra collected from the green layers of the three cross-sections (Fig. 3A, frequencies and their assignmentss listed in Table 2) present comparable spectral profiles, with vibrational features centered at: 946, 1050, 1350, 1442, 1598, 2855, 2935 cm^{-1}. These frequencies are in agreement with the presence of copper-based pigments, more commonly designated by the general term verdigris [4,5,11,48].

Specifically, the above mentioned Raman frequencies are in agreement with the characteristic bands of a copper acetate monohydrate ($Cu(CH_3COO)_2 \cdot H_2O$) [11].

The comparable spectra profiles observed in the three Raman spectra, may suggest that the copper-based pigments in the three objects share analogous chemical compositions and therefore comparable coordination geometries. Raman bands at 127, 196 and 457 cm^{-1} are attributed to lead-tin yellow type I, while the band at 1050 cm^{-1} is assigned to both the carbonate peak of lead white and to a copper acetate compound [41]. The presence of two broad bands in the OH region of samples L33_31 and L175_8, centered respectively at 3525 and 3636 cm^{-1}, could suggest the presence of basic copper acetates, though neutral copper acetates might be present as well [49]. The Raman feature at 1442 cm^{-1} is attributed to the COO^- symmetric stretching vibration of the acetate group of the copper compound, as reported in the literature [5,50]. Also, the bands centered at 1415–1420 cm^{-1} and at around 2935 cm^{-1} can be attributed to asymmetric deformation and stretching vibration of the methyl group, respectively [5,50], while the band at 1650 cm^{-1} may be assigned both to the stretching vibration of the olefinic group, $\nu(C{=}CH_2)$ [44,45,51], and to the OH bending of a basic copper chloride [11].

Raman bands at 947, 1088, 1298 cm^{-1} shared by the three samples can be associated to copper long-chain carboxylates, suggesting the presence of copper soaps [10,47].

The identification of mixtures of copper acetate complexes with lead-tin yellow type I and lead white is not surprising since it was quite common to mix copper-based compounds with lead-based pigments to obtain a specific range of shades [13,49,52]. Lead-tin oxides were a favorite on the artist's palette, because of their strong color and durability, but also because they accelerate the polymerization of oil paints [53–55].

Concerning the ATR-FTIR data collected from the green layers, their interpretation is particularly challenging, since the lead-based pigments absorption bands are centered in the same region of copper acetate complexes [13,42,56]. The ATR-FTIR spectra of the three samples

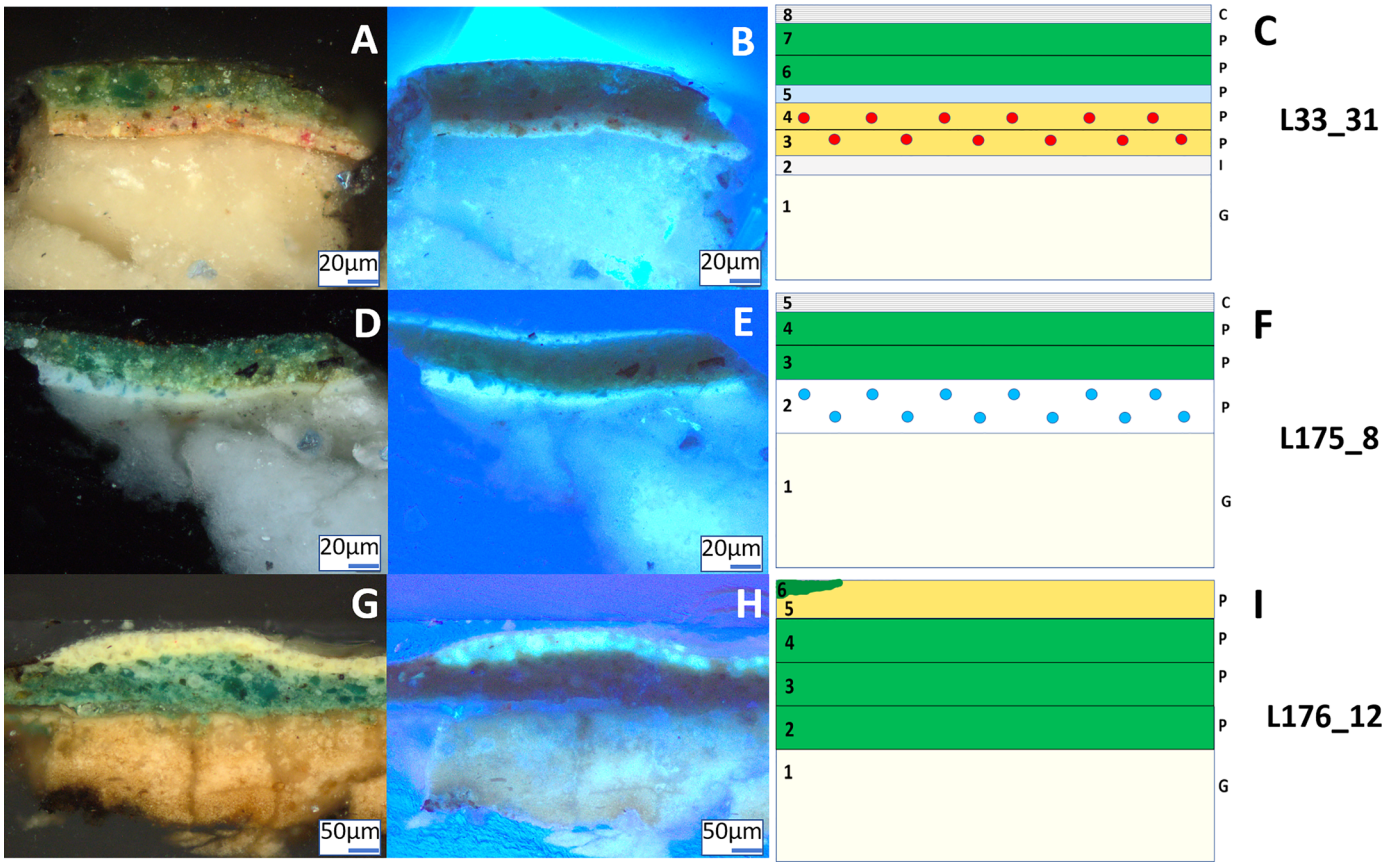

Fig. 2. Dark field (A-D-G) and UV micrographs (B-E-H) of the painting cross-sections L33_31 (A, B), L175_8 (D, E) and L176_12 (G, H). The stratigraphy and layers description (C, F, I) are reported for each cross-section (C: coating, P: paint, I: isolation, G: ground layer). The magnification of the micrographs is 20× and 50×. The thicknesses of the green paint layer are: around 40 µm for sample L33_31, around 40 µm for sample L175_8, and around 90 µm for sample L176_12.

(Fig. 3B) present different profiles. Specifically, the presence of copper acetate monohydrate and basic copper acetates has also been confirmed by these results, supporting and complementing the Raman spectral information [5,13]. The ATR-FTIR bands assigned to the copper acetate monohydrate are found at: 1050, 1350, 1444 and 1600 cm^{-1} [13,49], whereas characteristic bands for basic copper acetates are found respectively at: 872, 950, 1410, 1555, 1598 and 3445 cm^{-1} [49,56]

The band centered at around 1555 cm^{-1}, and observed in all the three samples, is assigned to the asymmetric stretching of the carboxyl group of the basic copper acetate compound [13]. In the OH region, two broad bands were found in the spectra of samples L175_8 and L176_12, centered at 3344 and 3375 cm^{-1}, respectively. Although, OH bands seem to be lacking in the spectrum of sample L33_31, this does not confirm the absence of hydroxyl groups or hydrated compounds [13]. In fact, in ATR geometry, the intensity of the OH bands is reduced in comparison to transmission measurements [13,57]. Furthermore, if the contact between the ATR crystal and the sample's surface is not optimal, the OH bands can be absent in the spectrum [58].

The absorption bands at 680 and 872 cm^{-1} are stretching vibrational modes of carbonate, attributed respectively to lead white and calcium carbonate [42]. The absorption mode at 1400 cm^{-1} is related to the carbonates [42].

In cross-section L176_12, the absorption band centered at 1585 cm^{-1} is characteristic of fatty acids copper carboxylates [10,13,42,56]. Also the band at 1435 cm^{-1}, found in sample L175_8, may be related to the CH_2 bending of a copper oleate [47]. No evidence of alteration products, such as copper formates (characteristic bands at 1374 and 3570 cm^{-1} [59]), were observed in these three samples. The band found at around 1320 cm^{-1} in samples L175_8 and L176_12 may be related to the COO^- symmetric stretching vibration of calcium oxalates or to copper oxalates [60], although the other fingerprint band at 1360 cm^{-1} is not appreciable in the spectrum, it might be masked by other bands. The vibrational mode at 1320 cm^{-1} could be also related to the presence of copper carboxylates [13]. In any case, the straightforward identification of alteration compounds such as copper oxalates, could be quite difficult with FTIR sometimes, particularly in presence of a mixture of pigments dispersed in an oily binding medium and with metal carboxylates [49]. The ester stretching bands at 1710–1728 cm^{-1}, together with the stretching bands of CH_2 and CH_3 groups at 2854 and 2925 cm^{-1}, indicate the use of an oily binder [13,42,56]. In the ATR-FTIR spectrum of sample L175_8 (Fig. 3B), the intensity ratio between the band attributed to COO^- and the stretching bands of CH_2 and CH_3 is particularly high, possibly due to cleavage reactions leading to volatile compounds, as previously reported in literature [61].

With EDX elemental analysis, chlorine was detected in both samples L175_8 and L176_12. This may suggest the presence of copper chlorides [62] and might also point to the use of honey and/or salts during manufacture [3] or the production of verdigris as *verde salsum* (a type of copper chloride) [62], such as that described by Theophilus [63]. On the other hand, chlorine was not observed in sample L33_31. In the SEM-EDX maps of both samples L175_8 and L176_12 (Figure S8), chlorine is not homogeneously distributed, but rather (this is more evident in sample L176_12) is concentrated in a few particles. This finding might support the hypothesis that the copper chlorides found in these samples are actually secondary products, formed by the interaction between copper compounds and the atmosphere, likely through cracks in the paint [21,49,64]. The absorption bands observed in the FTIR spectra of sample L176_12 and located at 856, 987, 3337 and 3345 cm^{-1} might be related to a copper(II) chloride hydroxide, such as

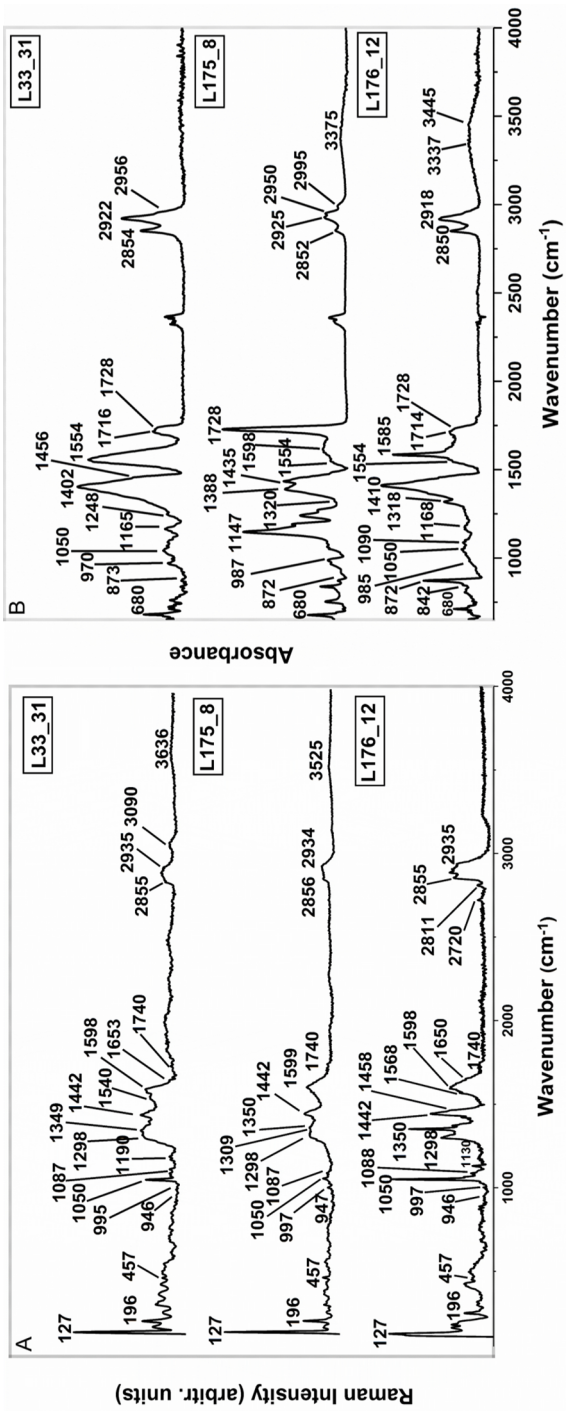

Fig. 3. 3A) Raman spectra collected from green layers, cross-sections L33_31 (layer 5 of the stratigraphy showed in Fig. 2), L175_8 (layer 5) and L176_12 (layer 4). The excitation line is at 785 nm. 3B) ATR-FTIR spectra collected in the green layers of cross-sections L33_31, L175_8 and L176_12.

atacamite and/or paratacamite ($Cu_2Cl(OH)_3$) [11,13,14]. In addition, lead soap aggregates have been often found to be considerably rich in chlorides [65]. However, further analyses (possibly by micro-diffraction) would be required to confirm the presence of these compounds.

Interestingly, the absorption band centered around 1554 cm^{-1} can be attributed to the shifting of the COO^- asymmetric stretching vibration, usually found around 1510 cm^{-1} in pure lead soaps [66]. This shifting to higher wavenumbers of the band, which in some cases is accompanied by a broadening, seems to be caused by the heterogenous nature of the aged oil paint. This is in turn characterized by the presence of different molecular species, such as different coordination environments of lead and carboxylic groups [66,67].

3.3. GC-MS investigation of the binding media

GC-MS analyses aided investigations related to the nature of the binding media in these samples. Analyses were carried out according to a tested analytical protocol [33]. Saccharide materials were not detected in any of the analyzed samples, while lipid and proteinaceous compounds were detected in several sub-samples as follows. Fig. 4 shows the selected ion monitoring (SIM) chromatograms of the amino acidic fractions and the lipid-resinous fractions of the samples.

All sub-samples showed the presence of proteinaceous material above the detection limit of the analytical procedure (Supplementary Material). The green paint layer of sample L33_31 (sub-sample L33_31_green) showed the presence of proteinaceous material between the LOD and LOQ of the same procedure, not allowing further identification of the binder's proteinaceous source. Table 3 reports the normalized amino acid content of the analyzed samples.

The high content of glycine, proline and the presence of hydroxyproline (molecular marker of collagen) [68,69] in the amino acid profiles, points to animal glue [70]. The presence of the latter in the ground layer, combined with chalk, is not surprising, since it was common practice in that period [71].

When looking at the results of the multivariate analysis, the sub-sample obtained from the preparation layer of sample L33_31 (Figure S9a), as well as the sub-samples from the green paint layer and the preparation layer obtained from sample L175_8 (Figure S9b), are located in the cluster of animal glue. Sample L176_12 (analyzed without sub-sampling), however, is not well located in any of the clusters, being shifted to higher values of PC1 (Figure S9c). This could be due to the contribution of a different proteinaceous material or to the degradation of the original one.

EGA-MS analyses (Figure S10) supported the GC-MS results allowing to identify, in the Total Ion Thermogram (TIT) of sample L175_8, the presence of fragment ions of diketopiperazines-DKPs (70, 111, 124, 154 m/z) and diketodipyrrole (186 m/z) characteristic of animal glue [72,73]. The TIT of sample L176_12 did not show signals ascribed to DKPs fragment ions, pointing to a high degradation of the proteinaceous material, thus preventing its direct identification [73]. However, fragmented ions ascribable to hexadecanenitrile and octadecanonitrile were not present in the TIT obtained not allowing for a further interpretation of the results obtained from the amino acid profile obtained by GC–MS. These molecules are known markers of egg yolk and they have already been identified in the pyrolytic profiles of highly aged and degraded paint samples such as the polychrome sculptures in clay from 6th century C.E. [72] and of Aegean-style wall painting dated to the end of 18th century B.C.E. [74]. Their presence in the pyrolytic profile of sample L176_12 would have allowed to ascertain the presence of a second proteinaceous material, suggested by the values of PC1 obtained, and identify it as egg. The residual fragments in the TITs are related to the presence of a lipid material (129, 239, 256 m/z).

The analysis of the lipid fraction showed the presence of a lipid material in all the analyzed samples with exception of sub-sample L175_8_prep. Fig. 4B shows the SIM chromatograms of the lipid-

Table 2
Characteristic Raman and IR bands of the spectra collected in the green paint-layers of samples L33_31, L175_8 and L176_12 and their assignments. In the table, vs, s, m, w, vw indicate very strong, strong, medium, weak, and very weak bands, respectively.

L33_31 Raman	L175_8 Raman	L176_12 Raman	Assignment	Attribution	L33_31 IR	L175_8 IR	L176_12 IR	Assignment	Attribution
127vs	127vs	127vs	ν(Pb-O) lattice mode	Lead tin yellow					
196m	196m	196m							
457w	457w	457w							
					680m	680m	680m	ν(CC)	Copper oleate/lead oleate/oleic acid
					758w	752w			
					837w	839m	842w	ν(CC)	
							856w	δ(OH)	Basic copper chlorides
					873w	872w	872m	δ(CH_2)/ ν(CC)	Basic copper acetates/linseed oil/metal carboxylates
946vw	947 vw	946 w	ν(CH_2)/ρ(CH_2)	Copper acetate monohydrate/Copper carboxylates		950vw	949vw	ν(CH_2)/ρ(CH_2)	Copper acetate monohydrate/ Basic copper acetates
1050m	1050w	1050s	δ(CH_3)/CO_3^{2-}	Copper acetate monoydrate/lead white?	1050w	1050w	1050w	δ(CH_3)/CO_3^{2-}	Copper acetate monohydrate/lead white?
1087w	1087vw	1088w	ν(CC)	Copper oleates	1095w		1090w	ν(CC)	Lead oleates/Oleic acid
		1130w	ν(CC)	Copper acetates/lead palmitates/ stearates					
1190w			δ(CH_2)	Lead oleates		1190sh		δ(CH_2)	Lead oleates
					1248w	1242m	1242vw	δ(CH_2)	Oleic acid
1298m	1298m	1298m	δ(CH_2)	Copper oleates					
	1309m					1320w	1318w	δ(CH_2)	Oleic acid
1349m	1349m	1350s	δ(CH_3)	Copper acetate monohydrate	1350sh		1350sh	δ(CH_3)	Copper acetate monohydrate
						1388m			
					1402vs		1410vs	CO_3^{2-}	Lead white
1442m	1442m	1442m	ν(COO^-)/ δ(CH_3)/ δ(CH_2)	Copper acetate monohydrate/copper oleates/lead oleates	1444sh	1442w	1444sh	δ(CH_2)	Copper acetate monohydrate/ Copper oleates/oleic acids
		1458sh			1456sh			δ(CH_2)	Metal carboxylates
1540m			ν_{as}(COO^-)	Lead carboxylates	1554s	1554w	1554sh	ν_{as}(COO^-)	Basic copper acetates/copper and lead carboxylates
		1568sh							
							1585s	ν_{as}(COO^-)	Copper carboxylates
1598m	1599m	1598m	ν(COO^-)	Copper acetate monohydrate/Copper carboxylates		1598w		ν_{as}(COO^-)	Copper acetate monohydrate/Basic copper acetates/neutral copper acetates/copper carboxylates
1653sh		1650sh	ν(C═C)/ ν(C═CH_2)/ δ(OH)	Copper oleates/basic copper chloride					
					1716m		1714m	ν(C═O)	Copper oleates/lead oleates/oleic acid
					1728m	1728vs	1728m		
1740vw	1740vw	1740vw	ν(C═O)	Linseed oil					
		2720w	ν(C−H) CH_2						
		2811w							
2855sh	2856w	2855m	ν(C−H) CH_2	Copper acetate monohydrate	2854m	2852w	2850m	ν_s(CH_2)	Copper oleate/lead oleate/oleic acid
					2922m	2925w	2918m	ν_{as}(CH_2)	
2935w	2934w	2935m	ν(C−H) CH_3						
					2956sh	2950w		ν_{as}(CH_3)	Copper acetate monohydrate/ Copper oleate/lead oleate/oleic acid
							2995w	ν(CH)	
							3337w	ν_{as}(O−H)	Basic copper chlorides
							3445w	ν_{as}(O−H)	Linseed oil/basic copper chloride/basic copper acetate
	3525vw			Basic copper acetates					
3636vw									

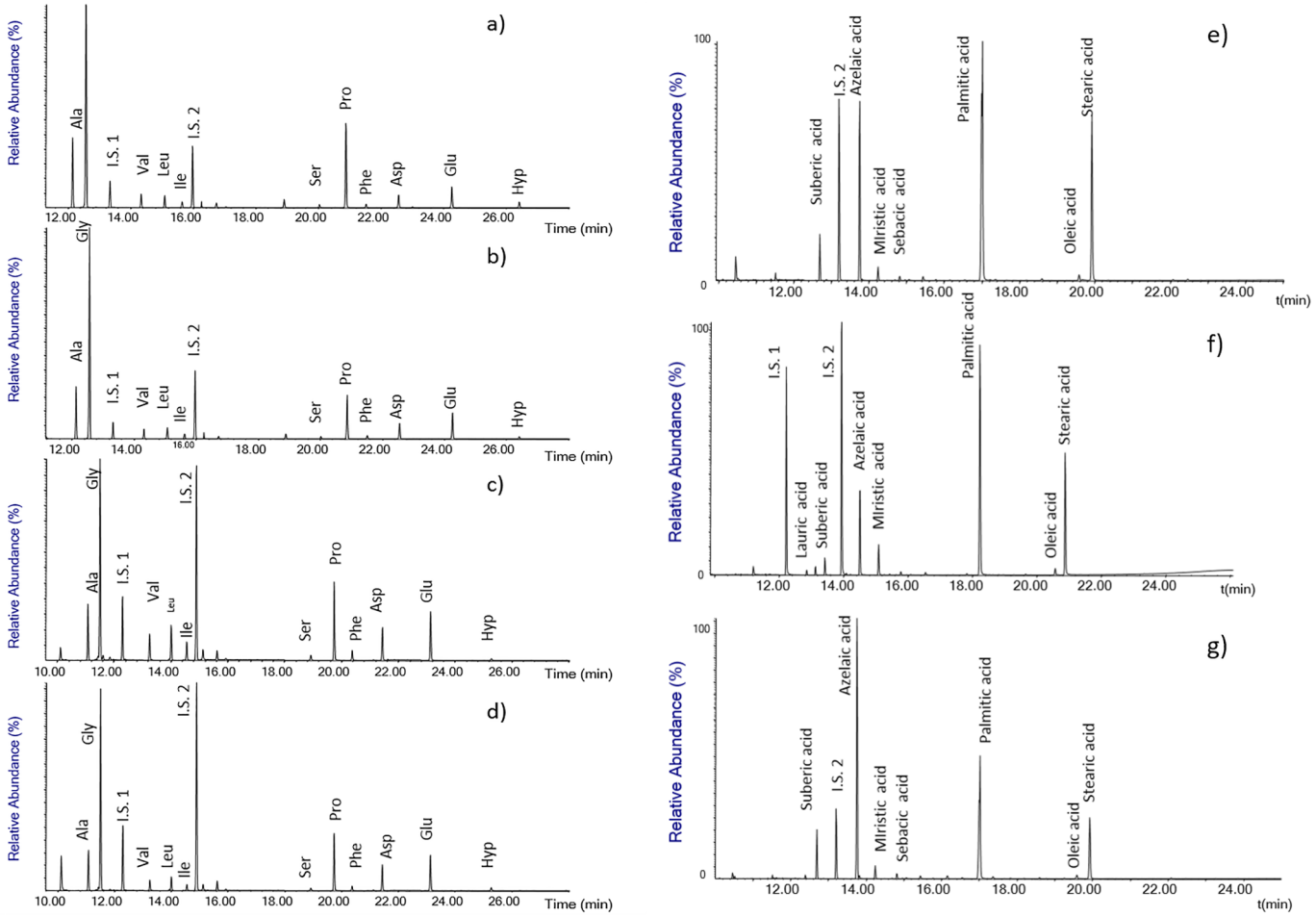

Fig. 4. Gas chromatograms acquired in SIM mode of the amino acidic fraction of a) L175_8 paint layers 3, 4, 5; b) L175_8 ground layer; c) L176_12; d) L33_31. I.S.1 and I.S.2 indicate hexadecane and norleucine (used as injection and derivatization internal standards, respectively). Ala: alanine; Gly: glycine; Val: valine; Leu: leucine; Ile: isoleucine; Ser: serine; Pro: proline; Phe: Phenylalanine; Asp: aspartic acid; Glu: glutammic acid; Hyp: hydroxyproline. Gas chromatograms acquired in SIM mode of the lipid-resinous fractions of the superficial paint layers of e) L33_31; f) L175_8; g) L176_12. I.S.1 and I.S.2 indicate hexadecane and tridecanoic acid (used as internal standards), respectively. Fatty acids were detected as trimethylsilyl derivatives.

resinous fraction of the sub-samples comprising the green paint layers.

Azelaic over palmitic acid ratio (A/P), palmitic over stearic acid ratio (P/S), oleic over stearic acid ratio (O/S) and the sum of the dicarboxylic acids (ΣD%) are shown in Table 4, as they are common parameters used in the characterization of lipid materials [75].

The values, calculated for the analyzed three samples, showed differences in the lipid material present. Results for sample L33_31 (both sub-samples obtained from the original sample, L33_31_green and L33_31_prep) show the characteristic parameters of a drying oil. The P/S ratio points to linseed oil. Results for sub-sample L175_8_green) are in agreement with the simultaneous presence of a drying oil and a non-drying lipid material (egg) while sub-sample L175_8_prep shows the presence of a lipid material below the LOQ of the procedure (Supplementary Material). Results for sample L176_12 also show the presence of a drying oil. However, the A/P ratio and the sum of dicarboxylic acids values point to a high oxidation degree of such drying oil [76,77], thus implying a degradation probably due to the raw material used or the conditions of preparation and ageing of the oil [76,77]. Di- or triterpenic resins were not detected in any of the samples. The presence of plant resins (Pinaceae resins, sandarac, mastic and dammar), animal resins (shellac), tar, pitches and natural waxes (beeswax, carnauba) was evaluated from the lipid-resinous fraction on

Table 4
Characteristic parameters used for the determination of the lipid material in the samples.

Sample	sub-sample	A/P	P/S	O/S	ΣD%
L33_31	green	1.1	0.9	0.1	31.7
	prep	1.7	0.8	0.1	43.2
L175_8	green	0.5	1.8	0.1	24.9
L176_12	bulk	4.1	1.4	0.2	71.2

Table 3
Normalized amino acid content of the samples.

Samples	Sub-sample	Ala	Gly	Val	Leu	Ile	Ser	Pro	Phe	Asp	Glu	Hyp
L33_31	prep	10.6	30.2	3.1	5.0	2.1	2.9	11.3	2.7	12.1	18.9	1.1
L175_8	green	18.0	33.2	3.3	3.1	1.7	1.3	19.7	2.3	5.2	8.9	3.3
	prep	9.8	28.4	2.3	3.5	1.6	1.7	10.8	2.9	9.3	22.2	7.4
L176_12	bulk	9.2	22.8	4.3	7.9	4.3	0.6	15.0	5.1	10.6	18.7	1.6

the basis of the occurrence of molecular markers, as reported in the literature [31–33].

3.4. GC-MS metal soaps analysis

In addition, samples L33_31, L175_8 and L176_12 were analyzed in bulk without sub-sampling with a procedure that allows the simultaneous detection and quantification of mixtures of free fatty acids and metal soaps in paint samples [29,30]. This procedure highlights significant differences between the hydrolyzed and the saponified fractions. Chromatograms are shown in Figure S11 (Supplementary material).

Results for samples L33_31 and L176_12 show the presence of free fatty acids (FFAs) and free dicarboxylic acids below the LOQ, whereas metal soaps were present in the samples above the LOQ. These results are in agreement with those observed in paint samples containing a drying oil and lead-based pigments. This data would support a possible mechanism of formation of metal soaps that does not involve hydrolysis of the triglycerides followed by reaction with the lead white [29].

The metal soap fractions of the samples show a substantial difference in terms of the relative amount of dicarboxylic acids. Although metal soaps of dicarboxylic acids are also present, results for sample L33_31 show a higher amount of metal carboxylates of saturated fatty acids, with palmitic acid being the most abundant one (A/P is around 0.5). Results from sample L176_12 show a higher relative amount of metal soaps from dicarboxylic acids, being azelaic the most abundant one, as demonstrated by the A/P ratio around 1.5. This evidence is consistent with the high oxidation degree of the lipid binder, as observed from the analysis of the lipid fraction. Sample L175_8, on the other hand, shows neither the presence of FFAs nor of metal soaps.

4. Conclusion

A summary, reporting the main analytical results for each sample, is presented in Table 5.

In this work, samples of green paints with similar stratigraphies from three late medieval painted wings were analyzed with complementary analytical techniques. Investigations allowed for the detection and identification of mixtures of basic copper acetates and copper acetate monohydrate in combination with lead-tin yellow type I and lead white. Metal soaps were also identified, specifically lead and copper carboxylates. Interestingly, the detection of chlorine in the green paint of samples L175_8 and L176_12 by SEM-EDX, and the discrimination of the characteristic Raman and ATR-FTIR bands of such compounds, confirms the presence of copper chlorides. The fact that this element appears not homogeneously distributed in the paint layer might suggest that these compounds formed likely as secondary products by the interaction between the copper compounds and the atmosphere, through cracks in the paint.

GC-MS analyses allowed the identification of both proteinaceous and lipid materials in the samples and supported the mentioned spectroscopic study.

In all the analyzed samples, animal glue has been identified. The analysis of sub-samples containing the ground layer (L33_31 prep, L175_8_prep) seems to point to the use of animal glue as a binder for the chalk-based ground layer. This is not surprising as this was standard in this period.

A drying oil was used in samples L176_12 and L33_31. While in sample L33_31 the drying oil was identified as linseed oil, the identification of the drying oil used in sample L176_12 was not straightforward. In the latter, a high degree of oxidation of the oil was observed. This might be related to the use of a different, unidentified, raw material or to a different treatment. This difference, in the ageing pathway, could be the reason behind the different degree of preservation of the panel paintings.

GC-MS investigations showed the presence of both drying and non-

Table 5
Summary of the analyses performed on the cross-section paint layers. C: coating, P: paint, I: isolation, G: ground layer. Refer to Fig. 2 to check the cross-section layer stratigraphy.

Sample	Paint layer	SEM-EDX	Raman	FTIR	GC-MS
L33_31	8 (C)				
	6–7 (P)	Cu, Pb, Sn	basic and neutral copper acetates, possible presence of lead carboxylates	basic and neutral copper acetates, possible presence of lead carboxylates, oil	Drying oil, metal carboxylates with a high content of saturated fatty acids
	5 (I)				
	3–4 (P)	Pb, Sn, Hg, S	vermilion, lead tin yellow type I		
	2 (I)				
	1 (G)	Ca, Sr, nano-fossils	chalk ($CaCO_3$)		Drying oil, proteinaceous material (animal glue)
L175_8	5(C)				Drying oil + non–drying lipid material (egg yolk? white egg?)
	3–4 (P)	Pb, Cu, Sn, Cl (secondary products?)	basic and neutral copper acetates, possible presence of lead carboxylates, copper oxalates calcium oxalates and copper chlorides	basic and neutral copper acetates, possible presence of lead carboxylates, copper oxalates, calcium oxalates and copper chlorides, oil	
	2 (P)	Cu, Pb, P	lead white, azurite	lead white, azurite	
	1 (G)	Ca, Sr, nano-fossils	chalk ($CaCO_3$)	chalk ($CaCO_3$), oil	Proteinaceous material (animal glue)
L176_12	6 (P)				unidentified drying oil showing high degree of oxidation, metal carboxylates of dicarboxylic acids, animal glue
	5 (P)	Sn, Pb	lead–tin yellow type I, lead carboxylates,	lead–tin yellow type I	
	4–3 (P)	Cu, Sn, Pb, Cl (secondary products?)	basic and neutral copper acetates, lead carboxylates, copper oxalates, copper chlorides and calcium oxalates	basic and neutral copper acetates, lead carboxylates, copper oxalates, copper chlorides and calcium oxalates, oil	
	2 (P)	Cu, Sn, Pb, Cl (secondary products?)	basic and neutral copper acetates, possible presence of lead carboxylate s, copper oxalates, copper chlorides and calcium oxalates	basic and neutral copper acetates, possible presence of lead carboxylates, copper oxalates, copper chlorides and calcium oxalates, oil	
	1 (G)	Ca, Sr, nano-fossils	chalk ($CaCO_3$)	chalk ($CaCO_3$), oil	

drying lipid material in sample L175_8. The presence of egg yolk or white egg found in mixture with a drying oil or used as a binder in the green or in the lead-white/azurite paint has not been confirmed by the data acquired. This evidence was also supported by the identification of phosphorus in the SEM-EDX maps of this sample.

GC-MS was helpful in identifying the presence of metal carboxylates, which, in presence of such a complex mixture of compounds, were very difficult to discriminate by vibrational spectroscopies. Metal soaps were detected in both samples L33_31 and L176_12. However, maybe because of the small amount of the analyzed sample, it cannot be excluded that sample L175_8 may have contained these compounds as well.

These differences in paint support claims that workshop practices could vary greatly among multiple painters who shared common patterns. While the panels from Bygland and Skjervøy (Fig. 1A and B) are similar in date, the paint formulations are quite different, pointing to different painters using the same workshop patterns. Understanding these differences was a primary goal of this study, which correlate to other data for the dates of the panels [28]. Another aim was to use these data for research on selective delamination of copper-green paints. Although from the collected data it was not possible to fully understand the process involved in this phenomenon, delamination might, however, be related to adhesion problems of the paint system caused for example by oil absorption into the chalk ground. In addition, the presence of organic isolation layers in sample L33_31, whose analysis was not possible because of their thinness, might have also a key role in the adhesion of the paint layers.

On the basis of the results of this study, future experiments will involve artificial weathering of paint reconstructions with the aim to understand the mechanisms of delamination, which affect many paintings in Scandinavian collections.

CRediT authorship contribution statement

Elena Platania: Conceptualization, Investigation, Data curation, Writing - original draft, Writing - review & editing, Visualization. **Noëlle L.W. Streeton:** Conceptualization, Project administration, Funding acquisition, Supervision, Writing - review & editing, Visualization. **Anna Lluveras-Tenorio:** Formal analysis, Validation, Investigation, Data curation, Writing - original draft, Writing - review & editing. **Anna Vila:** Investigation, Data curation, Resources, Writing - review & editing. **David Buti:** Investigation, Data curation, Resources, Writing - review & editing. **Francesco Caruso:** Data curation, Writing - original draft, Writing - review & editing. **Hartmut Kutzke:** Resources, Writing - review & editing. **Arne Karlsson:** Resources, Writing - review & editing. **Maria Perla Colombini:** Resources, Supervision. **Einar Uggerud:** Conceptualization, Resources, Supervision, Writing - review & editing.

Declaration of Competing Interest

The authors declare that they have no known competing financial interests or personal relationships that could have appeared to influence the work reported in this paper.

Acknowledgements

This project was supported by the Norwegian Research Council (project number: ES512866). We wish to thank Calin Costantin Steindal for access to the Raman instrumentation of the Saving Oseberg laboratories (KHM, University of Oslo). Authors wish also to thank Alessia Andreotti, Ilaria Bonaduce (University of Pisa) and Paz Arjonilla (Universidad de Jaén) for their kind assistance during the GC-MS analyses. This work was also partially carried out (University of Pisa) within the context of the JPI CMOP project: “Cleaning of modern oil paint” (Heritage Plus Joint Call project 2015e2018).

Supplementary materials

Supplementary material associated with this article can be found, in the online version, at doi:10.1016/j.microc.2020.104811.

References

[1] N. Eastaugh (Ed.), The Pigment Compendium: a Dictionary of Historical Pigments, Elsevier Butterworth-Heinemann, Amsterdam; Boston, 2004.
[2] A. Coccato, L. Moens, P Vandenabeele, On the stability of mediaeval inorganic pigments: a literature review of the effect of climate, material selection, biological activity, analysis and conservation treatments, Herit. Sci. 5 (2017).
[3] J.M. de la Roja, V.G. Baonza, M San Andrés, Application of Raman microscopy to the characterization of different verdigris variants obtained using recipes from old treatises, Spectrochim. Acta A Mol. Biomol. Spectrosc. 68 (2007) 1120–1125.
[4] T.D. Chaplin, R.J.H. Clark, D.A Scott, Study by Raman microscopy of nine variants of the green-blue pigment verdigris, J. Raman Spectrosc. 37 (2006) 223–229.
[5] M. San Andrés, J.M. de la Roja, V.G. Baonza, N Sancho, Verdigris pigment: a mixture of compounds. Input from Raman spectroscopy, J. Raman Spectrosc. 41 (2010) 1468–1476.
[6] Kühn H. Verdigris, Copper Resinate, Ashok Roy (Ed.), Archetype Publications Ltd, London, 2012.
[7] E. Platania, N.L.W. Streeton, H. Kutzke, A. Karlsson, E. Uggerud, N.H Andersen, Infrared, Raman and computational study of a crystalline mononuclear copper complex of relevance to the pigment Verdigris, Vib. Spectrosc. 97 (2018) 66–74.
[8] J.M. De la Roja, M. San Andrés, N.S. Cubino, S Santos-Gómez, Variations in the colorimetric characteristics of verdigris pictorial films depending on the process used to produce the pigment and the type of binding agent used in applying it, Color Res. Appl. 32 (2007) 414–423.
[9] D.A. Scott, Y. Taniguchi, E Koseto, The verisimilitude of verdigris: a review of the copper carboxylates, Stud. Conserv. 46 (2001) 73–91.
[10] V. Otero, D. Sanches, C. Montagner, M. Vilarigues, L. Carlyle, J.A. Lopes, et al., Characterisation of metal carboxylates by Raman and infrared spectroscopy in works of art, J. Raman Spectrosc. 45 (2014) 1197–1206.
[11] J. Buse, V. Otero, M Melo, New insights into synthetic copper greens: the search for specific signatures by Raman and infrared spectroscopy for their characterization in medieval artworks, Heritage 2 (2019) 1614–1629.
[12] S.A. Centeno, Identification of artistic materials in paintings and drawings by Raman spectroscopy: some challenges and future outlook: identification of artistic materials by Raman spectroscopy, J. Raman Spectrosc. 47 (2016) 9–15.
[13] S. Prati, I. Bonacini, G. Sciutto, A. Genty-Vincent, M. Cotte, M. Eveno, et al., ATR-FTIR microscopy in mapping mode for the study of verdigris and its secondary products, Appl. Phys. A 122 (2016).
[14] N. Salvadó, T. Pradell, E. Pantos, M.Z. Papiz, J. Molera, M.E. Seco, et al., Identification of copper-based green pigments in Jaume Huguet's Gothic altarpieces by Fourier transform infrared microspectroscopy and synchrotron radiation X-ray diffraction, J. Synchrotron Radiat. 9 (2002) 215–222.
[15] S. Švarcová, Z. Čermáková, J. Hradilová, P. Bezdička, D Hradil, Non-destructive micro-analytical differentiation of copper pigments in paint layers of works of art using laboratory-based techniques, Spectrochim. Acta A Mol. Biomol. Spectrosc. 132 (2014) 514–525.
[16] M.C. Caggiani, P. Colomban, Raman microspectroscopy for cultural heritage studies, Phys. Sci. Rev. 3 (2018).
[17] F. Pozzi, M. Leona, Surface-enhanced Raman spectroscopy in art and archaeology: SERS in art and archaeology, J. Raman Spectrosc. 47 (2016) 67–77.
[18] Casanova Municchia A., Micheli M., Ricci M.A., Toledo M., Bellatreccia F., Lo Mastro S., et al. Raman, SEM–EDS and XRPD investigations on pre-Columbian Central America “estucado” pottery. Spectrochim. Acta A Mol. Biomol. Spectrosc. 2016, 156:47–53.
[19] A. Nevin, J.L. Melia, I. Osticioli, G. Gautier, M.P Colombini, The identification of copper oxalates in a 16th century Cypriot exterior wall painting using micro FTIR, micro Raman spectroscopy and gas chromatography-mass spectrometry, J. Cult. Herit. 9 (2008) 154–161.
[20] F. Caruso, D.F. Chillura Martino, S. Saverwyns, M. Van Bos, L. Burgio, C. Di Stefano, et al., Micro-analytical identification of the components of varnishes from South Italian historical musical instruments by PLM, ESEM–EDX, microFTIR, GC–MS, and PY–GC–MS, Microchem. J. 116 (2014) 31–40.
[21] N. Salvadó, S. Butí, A. Labrador, G. Cinque, H. Emerich, T Pradell, SR-XRD and SR-FTIR study of the alteration of silver foils in medieval paintings, Anal. Bioanal. Chem. 399 (2011) 3041–3052.
[22] N.L.W. Streeton, Writing histories for late-medieval objects: the engagement of conservation with theoretical perspectives on material culture, Stud. Conserv. (2016) 1–13.
[23] Streeton N.L.W. Project description: after the Black Death: painting and polychrome sculpture in Norway, 1350–1550, Oslo: Norwegian Research Council. [Internet]. University of Oslo; 2013. Available from: http://www.hf.uio.no/iakh/english/research/projects/medieval-painting/index.html.
[24] A. Daly, N.L.W Streeton, Correction to: non-invasive dendrochronology of late-

medieval objects in Oslo: refinement of a technique and discoveries, Appl. Phys. A 124 (2018).
[25] N.L.W. Streeton, Perspectives (old and new) on late-medieval church art in Norway: questioning the hegemony of Lübeck workshops, Scand. Stud. 90 (2018) 50–77.
[26] C. Santoro, K. Zarkout, A.-S. Le Hô, F. Mirambet, D. Gourier, L. Binet, et al., New highlights on degradation process of verdigris from easel paintings, Appl. Phys. 114 (2014) 637–645.
[27] M. Vermeulen, J. Sanyova, K. Janssens, G. Nuyts, S. De Meyer, K De Wael, The darkening of copper- or lead-based pigments explained by a structural modification of natural orpiment: a spectroscopic and electrochemical study, J. Anal. At. Spectrom. 32 (2017) 1331–1341.
[28] A. Daly, N.L.W. Streeton, Non-invasive dendrochronology of late-medieval objects in oslo: refinement of a technique and discoveries, Appl. Phys. A 124 (2018) 246.
[29] J. La Nasa, F. Modugno, M. Aloisi, A. Lluveras-Tenorio, I Bonaduce, Development of a GC/MS method for the qualitative and quantitative analysis of mixtures of free fatty acids and metal soaps in paint samples, Anal. Chim. Acta 1001 (2018) 51–58.
[30] J. La Nasa, A. Lluveras-Tenorio, F. Modugno, I Bonaduce, Two-step analytical procedure for the characterization and quantification of metal soaps and resinates in paint samples, Herit. Sci. 6 (2018) 57.
[31] A. Andreotti, I. Bonaduce, M.P. Colombini, G. Gautier, F. Modugno, E Ribechini, Combined GC/MS analytical procedure for the characterization of glycerolipid, waxy, resinous, and proteinaceous materials in a unique paint microsample, Anal. Chem. 78 (2006) 4490–4500.
[32] I. Bonaduce, M. Cito, M.P Colombini, The development of a gas chromatographic–mass spectrometric analytical procedure for the determination of lipids, proteins and resins in the same paint micro-sample avoiding interferences from inorganic media, J. Chromatogr. A 1216 (2009) 5931–5939.
[33] A. Lluveras, I. Bonaduce, A. Andreotti, M.P Colombini, GC/MS analytical procedure for the characterization of glycerolipids, natural waxes, terpenoid resins, proteinaceous and polysaccharide materials in the same paint microsample avoiding interferences from inorganic media, Anal. Chem. 82 (2010) 376–386.
[34] S. Wold, K. Esbensen, P Geladi, Principal component analysis, Chemom. Intell. Lab. Syst. 2 (1987) 37–52.
[35] M. Ringnér, What is principal component analysis? Nat. Biotechnol. 26 (2008) 303–304.
[36] J.N. Miller, J.C. Miller, Statistics and Chemometrics for Analytical Chemistry, 6th ed., Prentice Hall, Harlow, 2010.
[37] I Jolliffe, Principal component analysis, in: M. Lovric (Ed.), Int Encycl Stat Sci. Springer Berlin Heidelberg, Berlin, Heidelberg, 2011, pp. 1094–1096.
[38] R. Bro, A.K Smilde, Principal component analysis, Anal. Methods 6 (2014) 2812–2831.
[39] R.G Brereton, Chemometrics, John Wiley & Sons, Ltd, Chichester, UK, 2003.
[40] V. Antunes, A. Candeias, J. Coroado, V. Serrão, M. Cachão, M.L Carvalho, A multidisciplinary approach to the study of the brightening effects of white chalk ground layers in 15th and 16th century paintings, Anal. Methods 8 (2016) 4785–4797.
[41] I.M. Bell, R.J.H. Clark, P.J Gibbs, Raman spectroscopic library of natural and synthetic pigments (pre- ≈ 1850 AD), Spectrochim. Acta A Mol. Biomol. Spectrosc. 53 (1997) 2159–2179.
[42] R. Mazzeo, S. Prati, M. Quaranta, E. Joseph, E. Kendix, M Galeotti, Attenuated total reflection micro FTIR characterisation of pigment–binder interaction in reconstructed paint films, Anal. Bioanal. Chem. 392 (2008) 65–76.
[43] A. Szkulmowska, M. Góra, M. Targowska, B. Rouba, D. Stifter, E. Breuer, et al., Applicability of optical coherence tomography at 1.55μm to the examination of oil paintings, in: J. Nimmrichter, W. Kautek, M. Schreiner (Eds.), Lasers Conserv Artworks, Springer Berlin Heidelberg, Berlin, Heidelberg, 2008, pp. 487–492.
[44] J. Mills, R. White, Organic Chemistry of Museum Objects, 2nd ed., Routledge, 2012.
[45] C.L. Higgitt, M. Spring, D.R Saunders, Pigment-medium interactions in oil paint films containing red lead or lead-tin yellow, Natl. Gallery Tech. Bull. 24 (2003) 75–95.
[46] E. Platania, N.L.W. Streeton, A. Vila, D. Buti, F. Caruso, E Uggerud, Investigation of mineralization products of lead soaps in a late medieval panel painting, Spectrochim. Acta A Mol. Biomol. Spectrosc. (2019) 117844.
[47] L. Robinet, M.C. Corbeil, The characterization of metal soaps, Stud. Conserv. 48 (2003) 23–40.
[48] J.M. De la Roja, M. San Andrés, N.S. Cubino, S Santos-Gómez, Variations in the colorimetric characteristics of verdigris pictorial films depending on the process used to produce the pigment and the type of binding agent used in applying it, Color Res. Appl. 32 (2007) 414–423.
[49] N. Salvadó, S. Butí, M. Cotte, G. Cinque, T Pradell, Shades of green in 15th century paintings: combined microanalysis of the materials using synchrotron radiation XRD, FTIR and XRF, Appl. Phys. A 111 (2013) 47–57.
[50] C. Conti, J. Striova, I. Aliatis, E. Possenti, G. Massonnet, C. Muehlethaler, et al., The detection of copper resinate pigment in works of art: contribution from Raman spectroscopy: detection of copper resinate pigment in works of art, J. Raman Spectrosc. 45 (2014) 1186–1196.
[51] C. Daher, C. Paris, A.-S. Le Hô, L. Bellot-Gurlet, J.-P Échard, A joint use of Raman and infrared spectroscopies for the identification of natural organic media used in ancient varnishes, J. Raman Spectrosc. 41 (2010) 1494–1499.
[52] M. Spring, New insights into the materials of fifteenth- and sixteenth-century Netherlandish paintings in the National Gallery, LOndon, Herit. Sci. 5 (2017).
[53] H Kühn, 4 Lead tin yellow, Stud. Conserv. 13 (1968) 7–33.
[54] H. Kühn, Verdigris and copper resinate, Stud. Conserv. 15 (1970) 12–36.
[55] C.S. Tumosa, M.F. Mecklenburg, The influence of lead ions on the drying of oils, Stud. Conserv. 50 (2005) 39–47.
[56] S. Prati, E. Joseph, G. Sciutto, R Mazzeo, New advances in the application of ftir microscopy and spectroscopy for the characterization of artistic materials, Acc. Chem. Res. 43 (2010) 792–801.
[57] M.R. Derrick, D. Stulik, J.M Landry, Infrared Spectroscopy in Conservation Science, Getty Conservation Institute, Los Angeles, 1999.
[58] S. Prati, G. Sciutto, E. Catelli, A. Ashashina, R Mazzeo, Development of innovative embedding procedures for the analyses of paint cross sections in ATR FITR microscopy, Anal. Bioanal. Chem. 405 (2013) 895–905.
[59] P. Ramamurthy, E.A. Secco, Studies on metal hydroxy compounds. XII. Thermal analyses, decomposition kinetics, and infrared spectra of copper basic oxysalts, Can. J. Chem. 48 (1970) 3510–3519.
[60] N. Salvadó, S. Butí, J. Nicholson, H. Emerich, A. Labrador, T Pradell, Identification of reaction compounds in micrometric layers from gothic paintings using combined SR-XRD and SR-FTIR, Talanta 79 (2009) 419–428.
[61] L. de Viguerie, P.A. Payard, E. Portero, Walter Ph, M Cotte, The drying of linseed oil investigated by Fourier transform infrared spectroscopy: historical recipes and influence of lead compounds, Prog. Org. Coat. 93 (2016) 46–60.
[62] M. Favaro, P.A. Vigato, A. Andreotti, M.P Colombini, La Medusa by Caravaggio: characterisation of the painting technique and evaluation of the state of conservation, J. Cult. Herit. 6 (2005) 295–305.
[63] Theophilus, De Diversibus Artis: The various Arts, Thomas Nelson & Sons, Oxford, 1961.
[64] D.A Scott, Bronze disease: a review of some chemical problems and the role of relative humidity, J. Am. Inst. Conserv. 29 (1990) 193–206.
[65] K Keune, Binding Medium, Pigments and Metal Soaps Characterised and Localised in Paint Cross Sections, University of Amsterdam, 2005 [Report of MOLART Series: MOLART11, AMOLF]. [Amsterdam].
[66] J.J. Hermans, K. Keune, A. Van Loon, M.J.N. Stols-Witlox, R.W. Corkery, P.D Iedema, The synthesis of new types of lead and zinc soaps: a source of information for the study of oil paint degradation, ICOM-CC 17th Trienn Conf Prepr Melb 15-19 Sept 2014 Ed J Bridg, Paris, International Council of Museums, 2014, p. 8.
[67] A. Lenz, L. Selegård, F. Söderlind, A. Larsson, P.O. Holtz, K. Uvdal, et al., ZnO nanoparticles functionalized with organic acids: an experimental and quantum-chemical study, J. Phys. Chem. C 113 (2009) 17332–17341.
[68] V. Rodwell, D Bender, Harpers Illustrated Biochemistry, 30th ed., McGraw Hill Professional, 2015.
[69] D.J Prockop, Collagens. Encycl Biol Chem. Elsevier, 2004, pp. 482–487.
[70] J.S. Mills, R. White, The Organic Chemistry of Museum Objects, 2nd ed., Reprinted, Butterworth-Heinemann, Oxford, 2006.
[71] S. Bucklow, R. Marks, L. Wrapson (Eds.), The Art and Science of the Church Screen in Medieval Europe: making, meaning, Preserving, The Boydell Press, Woodbridge, Suffolk, UK; Rochester, NY, 2017.
[72] S. Orsini, F. Parlanti, I Bonaduce, Analytical pyrolysis of proteins in samples from artistic and archaeological objects, J. Anal. Appl. Pyrolysis 124 (2017) 643–657.
[73] S. Sotiropoulou, G. Sciutto, A.L. Tenorio, J. Mazurek, I. Bonaduce, S. Prati, et al., Advanced analytical investigation on degradation markers in wall paintings, Microchem. J. 139 (2018) 278–294.
[74] I. Bonaduce, M.P. Colombini, Gas chromatography/mass spectrometry for the characterization of organic materials in frescoes of the Momumental Cemetery of Pisa (Italy), Rapid Commun. Mass Spectrom. 17 (2003) 2523–2527.
[75] A. Casoli, P.C. Musini, G Palla, Gas chromatographic-mass spectrometric approach to the problem of characterizing binding media in paintings, J. Chromatogr. A 731 (1996) 237–246.
[76] I. Bonaduce, L. Carlyle, M.P. Colombini, C. Duce, C. Ferrari, E. Ribechini, et al., New insights into the ageing of linseed oil paint binder: a qualitative and quantitative analytical study, in: M. Wanunu (Ed.), New insights into the ageing of linseed oil paint binder: a qualitative and quantitative analytical study, PLoS ONE 7 (2012) e49333.
[77] I. Bonaduce, L. Carlyle, M.P. Colombini, C. Duce, C. Ferrari, E. Ribechini, et al., A multi-analytical approach to studying binding media in oil paintings: characterisation of differently pre-treated linseed oil by DE-MS, TG and GC/MS, J. Therm. Anal. Calorim. 107 (2012) 1055–1066.